EXAFS Characterization of Dendrimer−Pt Nanocomposites Used for the Preparation of $Pt/\gamma\text{-}Al_2O_3$ Catalysts

Oleg S. Alexeev, Attilio Siani, Gwendoline Lafaye, Christopher T. Williams, Harry J. Ploehn, and Michael D. Amiridis*

Department of Chemical Engineering, University of South Carolina, Columbia, South Carolina 29208

Received: June 18, 2006; In Final Form: September 14, 2006

$Pt/\gamma\text{-}Al_2O_3$ catalysts were prepared using hydroxyl-terminated generation four (G4OH) PAMAM dendrimers as the templating agents and the various steps of the preparation process were monitored by extended X-ray absorption fine structure (EXAFS) spectroscopy. The EXAFS results indicate that, upon hydrolysis, chlorine ligands in the H_2PtCl_6 and K_2PtCl_4 precursors were partially replaced by aquo ligands to form $[PtCl_3(H_2O)_3]^+$ and $[PtCl_2(H_2O)_2]$ species, respectively. The results further suggest that, after interaction of such species with the dendrimer molecules, chlorine ligands from the first coordination shell of Pt were replaced by nitrogen atoms from the dendrimer interior, indicating that complexation took place. This process was accompanied by a substantial transfer of electron density from the dendrimer to platinum, indicating that the dendrimer plays the role of a ligand. Following treatment of the H_2PtCl_6/G4OH and K_2PtCl_4/G4OH complexes with $NaBH_4$, no substantial changes were observed in the electronic or coordination environment of platinum, indicating that metal nanoparticles were not formed during this step under our experimental conditions. However, when the reduction treatment was performed with H_2, the formation of extremely small platinum clusters, incorporating no more than four Pt atoms was observed. The nuclearity of these clusters depends on the length of the hydrogen treatment. These Pt species remained strongly bonded to the dendrimer. Formation of larger platinum nanoparticles, with an average diameter of approximately 10 Å, was finally observed after the deposition and drying of the H_2PtCl_6/G4OH nanocomposites on a $\gamma\text{-}Al_2O_3$ surface, suggesting that the formation of such nanoparticles may be related to the collapse of the dendrimer structure. The platinum nanoparticles formed appear to have high mobility because subsequent thermal treatment in O_2/H_2, used to remove the dendrimer component, led to further sintering.

Introduction

The performance of supported metal catalysts largely depends on the structure and composition of the metal particles and the nature of the support. Conventional methods used for the preparation of supported catalysts (e.g., incipient wetness, wet impregnation, or deposition-precipitation) involve the deposition of the metal precursors from solutions and often provide limited control over the structure of the resulting materials. Better uniformity of the supported metal particles has been achieved in the past through the use of organometallic molecular cluster precursors.[1] However, the issues of stability of such clusters on the surfaces of various supports, as well as difficulties in the synthesis and handling of the organometallic compounds during catalyst preparation steps, make the use of cluster-derived catalysts problematic for large-scale applications.

In recent years, alternative synthetic routes based on the use of templating agents, surfactants, or polymers have been proposed.[2] These efforts are based on the ability of such templating materials to stabilize various metal nanoparticles in solution. Among these templating materials, poly(amidoamine) (PAMAM) dendrimers have attracted growing attention. Dendrimers are quasispherical hyperbranched polymers incorporating various functional groups. They exhibit great structural and chemical versatility and can be tuned by controlling the core structure, the number, and type of the repeating units and the nature of the terminal functional groups.[3,4] The interior voids found in higher generation PAMAM molecules could accommodate metal nanoparticles, protecting them from aggregation until they are delivered to a support surface.

The use of dendrimers as templates for the synthesis of encapsulated nanoparticles is a relatively new field, with most of the reported data being related to homogeneous catalytic applications.[5,6] Since the first synthesis of dendrimer-stabilized Cu clusters was reported by Crooks and co-workers,[2] many different types of monometallic and bimetallic[7,8] metal−dendrimer nanocomposites have been successfully synthesized. The preparation of such metal−dendrimer nanocomposites bares similarities to the synthesis of colloids.[9] It involves the complexation of metal cations with interior tertiary amine[2,10] or amide groups,[10] which has been experimentally confirmed by NMR[10] and UV−visible[2] measurements. Once the complexation step is completed, a reducing agent (e.g., sodium borohydride or hydrogen) has been used to presumably reduce the metal cations to a zero valent state and form nanoparticles encapsulated within the dendrimer structure.[2,5,11−13] Published UV−visible,[2] TEM,[13] and SAXS[13] data appear to suggest the formation of metallic nanoparticles following this reduction step. Nevertheless, there is a lack of direct structural data in support of such a conclusion. Therefore, the question of whether the proposed templating mechanism is true remains open. Furthermore, little is known about the delivery of dendrimer-stabilized metal

* Corresponding author. E-mail: amiridis@engr.sc.edu. Telephone: 803 777 7294. Fax: 803 777 8265.

10.1021/jp063787+ CCC: $33.50
Published on Web 11/16/2006

nanoparticles onto surfaces. The ability to immobilize these nanocomposites onto high surface area metal oxide supports is a necessary step during the synthesis of heterogeneous catalysts.

The goal of this work is to acquire a better molecular-level understanding of the processes taking place during the synthesis of platinum−PAMAM nanocomposites used for the preparation of Pt/γ-Al_2O_3 catalysts. We are reporting, for the first time, precise structural characterization of platinum−PAMAM dendrimer nanocomposites by X-ray absorption fine structure (EXAFS) spectroscopy. These measurements enabled us to evaluate the local environment of platinum during the various preparation steps. In particular, we used EXAFS to characterize (1) $H_2PtCl_6 \cdot 6H_2O$ and K_2PtCl_4 precursor solutions in water, (2) solutions of Pt^{n+} cations complexed with a fourth-generation hydroxyl-terminated (G4OH) PAMAM dendrimer, (3) the same solutions following treatment with reducing agents, (4) these platinum−PAMAM nanocomposites deposited onto a γ-Al_2O_3 surface, and (5) the resulting materials following thermal treatment to remove the dendrimer component.

Experimental Section

Reagents and Materials. The hydroxyl-terminated generation four (G4OH) poly(amidoamine) (PAMAM) dendrimer was purchased as a 10% solution in methanol (Aldrich). Prior to use, the methanol was removed under N_2 flow at room temperature, and a 0.17 mM aqueous solution of G4-OH dendrimer was prepared. Milli-Q deionized water (18 MΩ·cm) was used to prepare all aqueous solutions. $H_2PtCl_6 \cdot 6H_2O$ (99.95% purity, Alfa Aesar) and K_2PtCl_4 (99.9% purity, Aldrich) were used as supplied. Powdered γ-Al_2O_3 (Alfa Aesar) with a BET surface area of 45 m^2/g was calcined in air for 4 h at 500°C prior to use. UHP grade H_2 and N_2 (National Welders) were additionally purified from traces of moisture and oxygen by passage through appropriate traps (Agilent, models GMT-2GCHP and OT-3, respectively).

Preparation of G4OH−Pt_{40}. The preparation of metal−dendrimer nanocomposites has been reported previously.[2,7,8] In brief, an appropriate amount of a 25.6 mM aqueous solution of the desired platinum precursor was added under nitrogen flow to a 0.17 mM aqueous solution of G4OH dendrimer in order to obtain a molar ratio of Pt to G4OH dendrimer equal to 40. The mixture was stirred under nitrogen flow for 3 days to allow the complexation of Pt^{n+} cations in the solution with interior functional groups of the dendrimer. The resulting complex is denoted as G4OH−$(Pt^{n+})_{40}$ for simplicity. After the complexation was completed, the solution was dialyzed using a benzoylated cellulose dialysis sack having a molecular weight cutoff of 2000 to remove impurities. During subsequent reduction treatments, either H_2 was bubbled into the dialyzed solution or a fresh aqueous solution of $NaBH_4$ (ratio of BH_4^- to Pt of 8:1) was slowly added. Both treatments were performed at room temperature. Following these steps, the resulting solutions were used for further preparation or characterization without additional purification.

Preparation of G4OH−$(Pt^{n+})_{40}$/γ-Al_2O_3. Supported samples were prepared by slurrying of a G4OH−$(Pt^{n+})_{40}$ solution with γ-Al_2O_3 in amounts chosen to yield samples containing 1 wt. % Pt. The excess water was removed by slow evaporation at room temperature, followed by evacuation at room temperature. The resulting solid samples were finally treated in an O_2/He mixture at 400 °C for 1 h followed by H_2 at 300 °C for 2 h to remove the dendrimer component.

EXAFS Spectroscopy. EXAFS spectra were collected at beamline X-18B at the National Synchrotron Light Source (NSLS), Brookhaven National Laboratory, Upton, NY, and at beamline 2-3 at the Stanford Synchrotron Radiation Laboratory (SSRL), Stanford Linear Accelerator Center, Menlo Park, CA. The storage ring electron energy was 2.8 GeV at NSLS and 3 GeV at SSRL. The ring currents were 110−250 and 50−100 mA at NSLS and SSRL, respectively.

TABLE 1: Crystallographic Data and Fourier Filtering Ranges Used for Reference Compounds[a]

	crystallographic data			Fourier transform		
sample	shell	N	R (Å)	Δk ($Å^{-1}$)	Δr (Å)	n
Pt foil	Pt−Pt first	12	2.77	1.9−16.5	1.9−3.0	3
	Pt−Pt third	24	4.80	1.9−16.5	4.17−4.90	3
	Pt−Pt fourth	12	5.54	1.9−16.5	4.90−5.98	3
$Na_2Pt(OH)_6$	Pt−O	6	2.05	1.4−16.5	0.5−2.0	3
K_2PtCl_4	Pt−Cl	4	2.31	1.9−15.9	1.0−2.7	3
$Pt(NH_3)_4Cl_2$	Pt−N	4	2.05	2.9−15.9	0.9−2.1	3
$Ir_4(CO)_{12}$	Ir−C(Pt−C)	3	1.87	2.8−16.5	1.1−2.0	3

[a] Notation: N, coordination number for absorber-backscatterer pair; R, distance; Δk, limits used for forward Fourier transform (k is the wave vector); Δr, limits used for the shell isolation (r is the distance); n, power of k used for Fourier transformation.

The G4OH−$(Pt^{n+})_{40}$/γ-Al_2O_3 samples were loaded as wafers into an in situ EXAFS cell[14] connected to a gas distribution system, allowing for the treatment of the samples with various gases. After a desired treatment was completed, the EXAFS cell was evacuated at room temperature to 10^{-5} Torr, cooled to nearly liquid nitrogen temperature, and aligned in the X-ray beam. The EXAFS data were recorded in the transmission mode with an appropriate amount of sample to give an absorbance of approximately 2.5 at the Pt L_3 (11563.7 eV) edge.

Data for the aqueous solutions were recorded in the fluorescence mode with a 13th element Ge detector. The total count rate for the Ge detector was in the range of 30 000−40 000 counts/s. It was experimentally established that the detector readings are linear within this range and no corrections for the dead time are required. Liquid samples were loaded into an in situ EXAFS cell designed to allow handling of samples without air exposure.[15] The data were collected at room temperature with a Si(111) double-crystal monochromator that was detuned by 40% to minimize the effects of higher harmonics in the X-ray beam.

The EXAFS data were analyzed with experimentally determined reference files obtained from EXAFS data characterizing materials of known structure. The Pt−Pt, Pt−O, Pt−Cl, and Pt−N interactions were analyzed with phase shifts and backscattering amplitudes obtained from EXAFS data characterizing platinum foil, $Na_2Pt(OH)_6$, K_2PtCl_4, and $Pt(NH_3)_4Cl_2$, respectively. When it was necessary to analyze higher Pt−Pt shells, the second shell was analyzed with a phase shift and backscattering amplitude obtained for the first shell of Pt foil. However, the 3rd and 4th Pt−Pt shells are strongly effected by multiple scattering as a consequence of the linearity of Pt−(Pt)−Pt moieties, and it is necessary to fit these contributions with phase shifts and backscattering amplitudes obtained from a reference also exhibiting multiple scattering.[16] Therefore, the 3rd and 4th Pt−Pt shell contributions were analyzed with phase shifts and backscattering amplitudes extracted for the 3rd and 4th shells of Pt foil, respectively. The Pt−C contributions were analyzed with phase shifts and backscattering amplitudes obtained from EXAFS data characterizing crystalline $Ir_4(CO)_{12}$, which has only terminal CO ligands. The transferability of the phase shifts and backscattering amplitudes characterizing platinum and iridium, which are near neighbors in the periodic table, has been justified experimentally.[17,18] The crystallographic coordination parameters

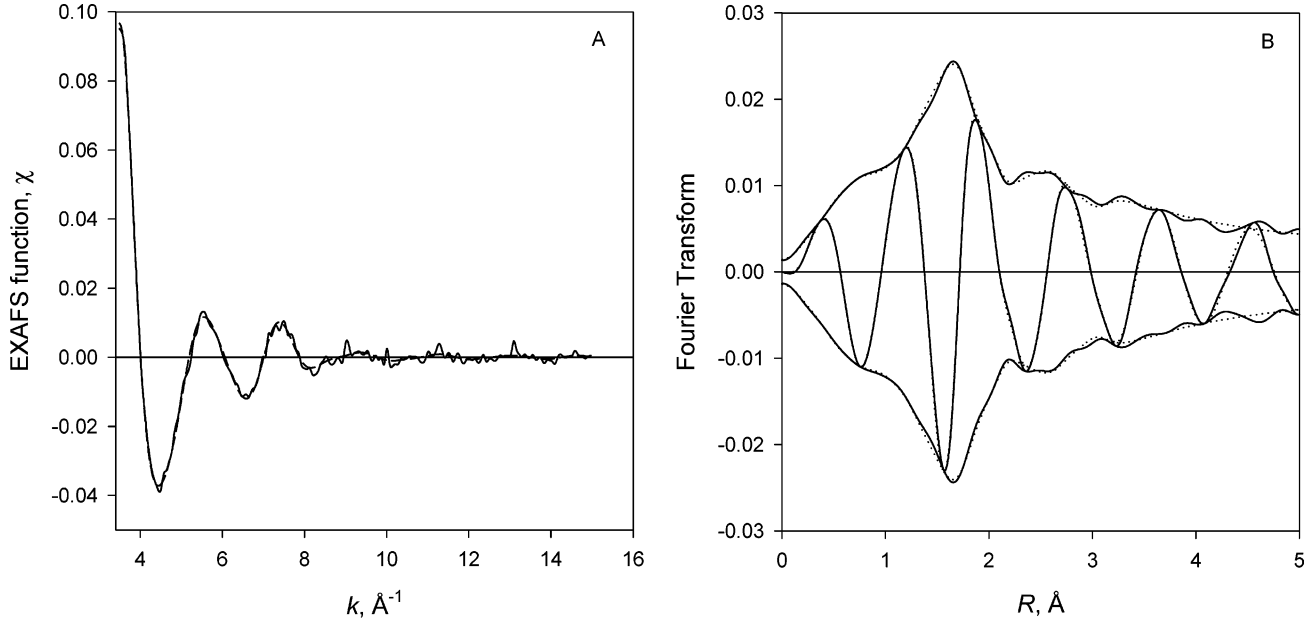

Figure 1. Results of EXAFS analysis characterizing G4OH−$(Pt^{2+})_{40}$ complexes formed during the interaction of K_2PtCl_4 with G4OH in an aqueous solution: (A) experimental EXAFS (χ) function (solid line) and sum of the calculated contributions as stated in Table 5 (dashed line); (B) imaginary part and magnitude of uncorrected Fourier transform (k^0 weighted, $\Delta k = 3.5-15.0$ Å^{-1}) of experimental EXAFS data (solid line) and sum of the calculated contributions as stated in Table 5 (dotted line).

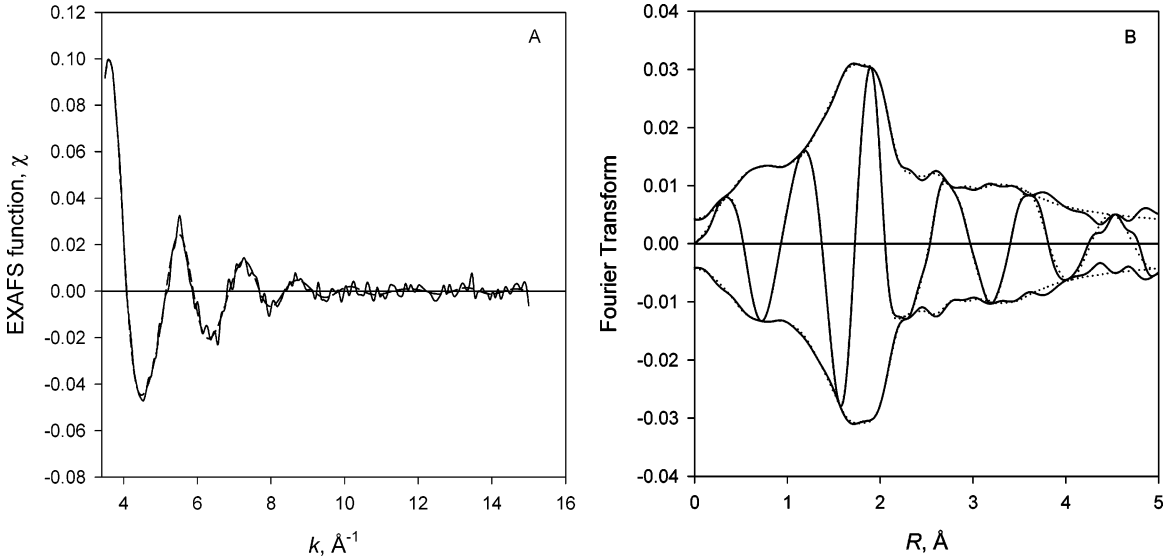

Figure 2. Results of EXAFS analysis characterizing G4OH−$(Pt^{4+})_{40}$ complexes formed during the interaction of H_2PtCl_6 with G4OH in an aqueous solution: (A) experimental EXAFS (χ) function (solid line) and sum of the calculated contributions as stated in Table 3 (dashed line); (B) imaginary part and magnitude of uncorrected Fourier transform (k^0 weighted, $\Delta k = 3.5-15.0$ Å^{-1}) of experimental EXAFS data (solid line) and sum of the calculated contributions as stated in Table 3 (dotted line).

for all the reference compounds, the weighting of the Fourier transform, and the ranges in k and r space used to extract the reference functions from the experimental EXAFS data are given in Table 1. The EXAFS parameters were extracted from the raw data with the aid of the XDAP software.[19] The methods used to extract the EXAFS function from the raw data are essentially the same as those reported elsewhere.[20] The data used for each sample were the averages of five scans.

The data at the Pt L_3 edge were analyzed with a maximum of 24 free parameters over the ranges of $3.50 < k < 15.50$ Å^{-1} (where k is the wave vector) and $0.0 < r < 5.0$ Å (where r is the distance from the absorbing Pt atom). The statistically justified number of free parameters, n, was found to be 39, as estimated on the basis of the Nyquist theorem:[21,22] $n = (2\Delta k \Delta r/\pi) + 1$, where Δk and Δr respectively are the k and r ranges used in the data fitting.

The parameters characterizing both the high-Z (Pt−Pt) and low-Z (Pt−N, Pt−C, Pt−O, Pt−Cl) contributions for the different samples examined were determined by multiple-shell fitting in r-space with application of k^1 and k^3 weighting in the Fourier transformations.[20] The fit was optimized by use of a difference file technique with phase- and amplitude-corrected Fourier transforms of the data.[23,24] The parameters determined by this fitting routine are summarized in Tables 2−8, and comparisons of the data and fits in r-space for selected samples are shown in Figures 1−4.

Standard deviations reported in these tables for the various parameters were calculated from the covariance matrix, taking into account the statistical noise of the EXAFS data and the correlations between the different coordination parameters as described elsewhere.[25] Systematic errors are not included in the calculation of the standard deviations. The values of the

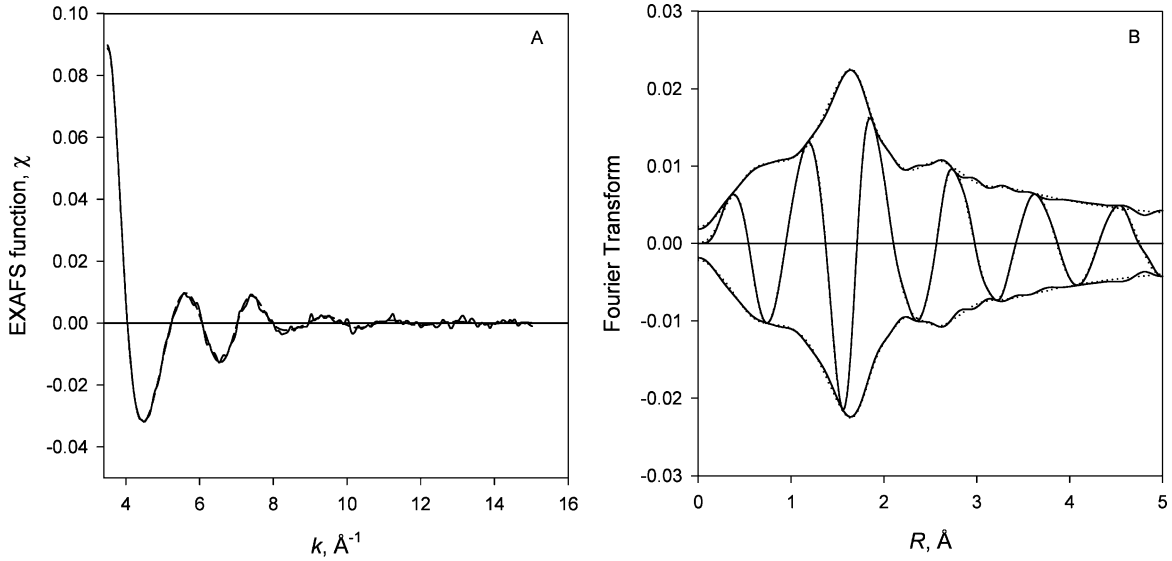

Figure 3. Results of EXAFS analysis characterizing G4OH−$(Pt^{2+})_{40}$ complexes treated with $NaBH_4$ in an aqueous solution: (A) experimental EXAFS (χ) function (solid line) and sum of the calculated contributions as stated in Table 6 (dashed line); (B) imaginary part and magnitude of uncorrected Fourier transform (k^0 weighted, $\Delta k = 3.5-15.0$ Å^{-1}) of experimental EXAFS data (solid line) and sum of the calculated contributions as stated in Table 6 (dotted line).

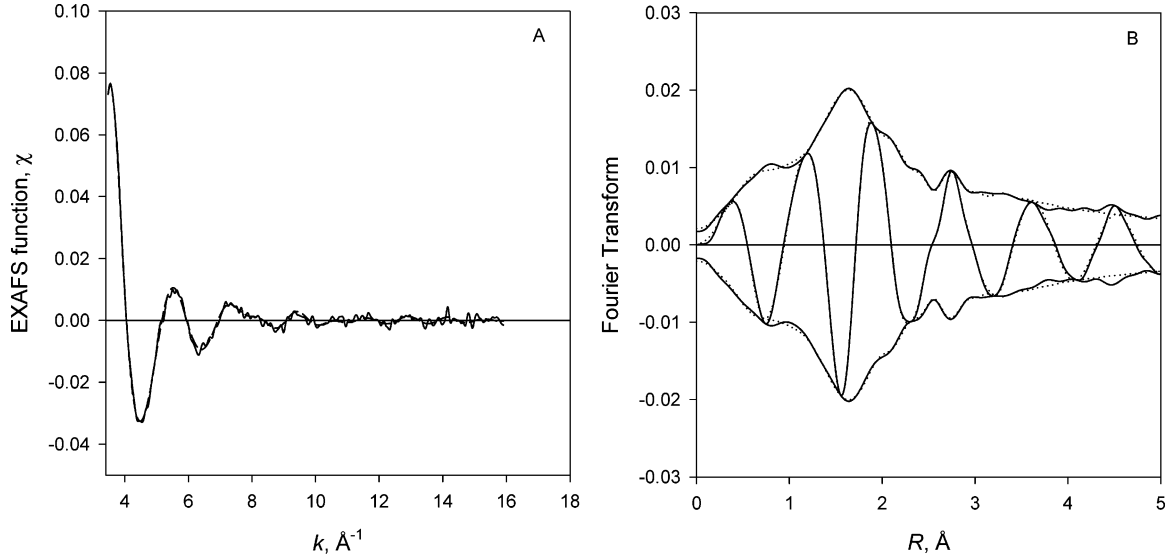

Figure 4. Results of EXAFS analysis characterizing G4OH−$(Pt^{4+})_{40}$ complexes treated with $NaBH_4$ in an aqueous solution: (A) experimental EXAFS (χ) function (solid line) and sum of the calculated contributions as stated in Table 6 (dashed line); (B) imaginary part and magnitude of uncorrected Fourier transform (k^0 weighted, $\Delta k = 3.5-15.0$ Å^{-1}) of experimental EXAFS data (solid line) and sum of the calculated contributions as stated in Table 6 (dotted line).

goodness of fit (ϵ_ν^2) were calculated as outlined in the *Reports on Standards and Criteria in XAFS Spectroscopy*.[26] The variances in both the imaginary and absolute parts were used to determine the fit quality.[27]

XANES Measurements and Analysis. X-ray absorption near-edge (XANES) spectra of each sample were also obtained during the X-ray absorption measurements described above. Normalized XANES spectra were obtained by subtracting the pre-edge background from the raw data with a modified Victoreen equation and by dividing the absorption intensity by the height of the absorption edge. The band structure curves were numerically integrated using the XDAP software.[19]

Results and Discussion

Structural Characterization of H_2PtCl_6 and K_2PtCl_4 in Aqueous Solutions. Hydrogen hexachloroplatinate (IV) (H_2PtCl_6) is known to undergo a series of hydrolysis reactions in aqueous solutions, while the octahedral coordination of Pt(IV) remains intact.[28] The exact pathway for the hydrolysis of H_2PtCl_6 has been discussed in the literature.[28−31] In general, it can be described as follows. Chloride anions are first replaced by water molecules during hydrolysis of some Pt−Cl bonds, leading to the formation of $[PtCl_{6-x}(H_2O)_x]^{-2+x}$ complexes. The ligand exchange of Cl^- ions by H_2O can then be followed by a slow H_2O-OH^- exchange reaction during which $[PtCl_{6-x}(OH)_y(H_2O)_{x-y}]^{-2+x-y}$ complexes are formed. The exact type and structure of the species formed during these hydrolysis reactions strongly depends on the solution pH and the concentrations of H_2PtCl_6 and chloride ions.[28] As a result, the structure of H_2PtCl_6 in aqueous solutions is expected to be different from that of solid H_2PtCl_6 in which only the presence of Pt−Cl contributions is expected.

Our EXAFS data for an aqueous solution containing 200 ppm of H_2PtCl_6 at a pH of approximately 2.7 indicate that the first

TABLE 2: Structural Parameters Characterizing H_2PtCl_6 and K_2PtCl_4 in an Aqueous Solution[a]

sample	shell	N	R (Å)	$\Delta\sigma^2$ (Å^2)	ΔE_0 (eV)	ϵ_ν^2	k^1 variances (%) im.	abs
H_2PtCl_6/H_2O	Pt−Cl	3.0	2.31	0.00590	−2.0	3.2	0.98	0.54
	Pt−O_1	3.2	2.01	0.00360	12.8			
	Pt−O_2	4.5	3.77	0.00290	−0.6			
K_2PtCl_4/H_2O	Pt−Cl	2.1	2.33	−0.00086	−7.4	2.6	0.81	0.42
	Pt−O_1	2.2	2.17	−0.00008	−6.7			
	Pt−O_2	4.7	3.81	0.00572	−0.9			

[a] Notation: R-space fit: $\Delta k = 3.5-15.0$ Å^{-1}, $\Delta r = 1.0-4.5$ Å; standard deviations in fits: $N \pm 20\%$, $R \pm 1\%$, $\Delta\sigma^2 \pm 5\%$, $\Delta E_0 \pm 10\%$; N, coordination number; R, distance between absorber and backscatterer atoms; $\Delta\sigma^2$, the Debye−Waller factor, which is relative to the Debye−Waller factor of the reference compound; ΔE_0, the inner potential correction accounts for the difference in the inner potential between the sample and the reference compound; ϵ_ν^2, goodness of fit. The Pt−O_1 and Pt−O_2 contributions represent the first and the second salvation shells, respectively.

coordination shell of Pt consists on average of three chlorine atoms at a Pt−Cl distance of 2.31 Å and three oxygen atoms at a Pt−O distance of 2.01 Å (Table 2). The observed Pt−O contributions in this case represent aquo ligands (i.e., H_2O or OH^-), and the bond distances obtained are in good agreement with those reported earlier for aqueous $[Pt(H_2O)_4]^{2+}$ species.[32,33] Therefore, these structural parameters indicate that, upon hydrolysis of H_2PtCl_6, approximately three chlorine ligands per Pt complex are replaced by the solvent to form $[PtCl_3(H_2O)_3]^+$, which becomes the predominant species in the solution. This conclusion is consistent with earlier reports postulating the formation of such species at similar concentrations and acidity.[28] Because EXAFS provides average structural information, the data may alternatively suggest that none of the $[PtCl_{6-x}(H_2O)_x]^{-2+x}$ species is really dominant in water solution under the conditions examined. Provided that substitutions of Cl^- by H_2O can take place simultaneously for up to six Cl^- ions, in the event of equal concentrations of the various partially hydrolyzed species in solution, the calculated Pt−Cl and Pt−O coordination numbers would on average be equal to three for both contributions, as observed in our data (Table 2).

Similarly to $PtCl_6^{2-}$, the planar square $PtCl_4^{2-}$ complex also undergoes hydrolysis in aqueous solutions, leading to the formation of $[PtCl_{4-x}(H_2O)_x]^{x-2}$ species.[32] Once again, the type of species formed strongly depends on the solution pH and the concentrations of K_2PtCl_4 and chloride ions.[34] Our EXAFS data collected for an aqueous solution containing 1500 ppm of K_2PtCl_4 at a pH of approximately 4.3 indicate that the first coordination shell of Pt consists on average of two chlorine atoms at a Pt−Cl distance of 2.33 Å and two oxygen atoms at a Pt−O distance of 2.17 Å (Table 2). Similar to the case of H_2PtCl_6, the observed Pt−O contributions in this case represent aquo ligands, and the calculated structural parameters indicate that, during hydrolysis of K_2PtCl_4, an average of two chlorine ligands per Pt complex are replaced by the solvent. Once again, the data suggest that either the $[PtCl_2(H_2O)_2]$ complex is the dominant species under these conditions, or all four partially hydrolyzed complexes exist in approximately equal concentrations.

In addition to the first-shell Pt−O_1 contributions representing the aquo ligands, Pt−O_2 contributions were also observed for both precursors at a distance of approximately 3.77−3.81 Å. These contributions represent interactions between water molecules of the second solvation shell with the $[PtCl_{6-x}(H_2O)_x]^{x-2}$ and $[PtCl_{4-x}(H_2O)_x]^{x-2}$ units, similar to those reported elsewhere.[32]

Interaction of H_2PtCl_6 and K_2PtCl_4 with G4OH Dendrimers. When an aqueous solution of H_2PtCl_6 is brought in contact with the G4OH dendrimer, complexation of the Pt^{4+} ions with the dendrimer's functional groups is expected to take place. On the basis of the blue-shift of the characteristic amide bands in the FTIR spectra of G4OH−$(Pt^{n+})_{40}$, it has been suggested that the amide groups of the dendrimer participate in this complexation.[35] Furthermore, NMR data reported previously[10] indicate that tertiary amines and amides are capable of coordinating Pt^{n+} cations. The degree of Pt^{n+} complexation with these functional groups depends largely on the nature and generation of the dendrimer because steric crowding of functional groups may occur in higher generation dendrimers.[10] On the basis of these reports, it is reasonable to assume then that if complexation of $[PtCl_{6-x}(H_2O)_x]^{x-2}$ and $[PtCl_{4-x}(H_2O)_x]^{x-2}$ units with the dendrimer were to take place, the first coordination shell of Pt would include both oxygen (representing the aquo ligands) and nitrogen (representing the dendrimer's functional groups) atoms.

The distinction between nitrogen and oxygen backscatterers with EXAFS is problematic because these two elements are neighbors in the periodic table and it is generally assumed that the phase shifts and backscattering amplitudes are transferable among the nearest neighbors for the whole periodic table.[36] It is very common, for example, to analyze metal−nitrogen contributions with references obtained from the corresponding metal oxides without distinguishing between nitrogen and oxygen neighbors.[37,38] However, it has also been shown that Pt−N and Pt−O phase shifts and backscattering amplitudes experimentally obtained from the EXAFS spectra of $Na_2Pt(OH)_6$ and $Pt(NH_3)_4(OH)_2$ reference compounds have small but significant differences.[39] For example, the backscattering amplitude function for Pt−N is somewhat smaller than that for Pt−O. As a result, when both Pt−N and Pt−O contributions are present in an EXAFS spectrum, the use of a Pt−O reference to model Pt−N contributions leads to underestimation of the Pt−N coordination numbers.[40] Similarly, the use of a Pt−N reference to model Pt−O contributions would result in overestimated parameters.[40] It has also been reported that the phase shift functions for Pt−O and Pt−N have a difference of more than 2π radians depending on k.[39] Consequently, models that include both Pt−N and Pt−O contributions can describe the experimental results better than models with only one Pt−O (or Pt−N) shell, as demonstrated elsewhere.[39]

We first consider the G4OH−$(Pt^{4+})_{40}$ complex formed during the interaction of H_2PtCl_6 and G4OH. Taking into account the difficulties described above in separating the Pt−O and Pt−N contributions expected to be present in the spectra, we took under consideration various models based on the assumption that only oxygen, only nitrogen, or both oxygen and nitrogen neighbors are present in the first coordination shell of platinum. The best fit parameters calculated for all these models are summarized in Table 3. The data of Table 3 clearly indicate that these structural models cannot be distinguished based solely on the statistical analysis parameters because the goodness of fit (ϵ_ν^2) and variances for the imaginary (im.) and absolute (abs) parts of the Fourier transform values are all in the acceptable range and only slightly differ from model to model. However, all three models indicate that, on average, only two chlorine ligands remained in the first coordination shell of platinum after the complexation, which is consistent with the suggestion that, during complexation, some chlorine ligands were replaced by

TABLE 3: Structural Parameters Characterizing Interactions of H_2PtCl_6 with a G4OH Dendrimer in an Aqueous Solution[a]

							k^1 variances (%)	
sample	shell	N	R (Å)	$\Delta\sigma^2$ (Å^2)	ΔE_0 (eV)	ϵ_ν^2	im.	abs
fit parameters assuming that only oxygen neighbors are present								
G4OH−$(Pt^{4+})_{40}$	Pt−Cl	2.2	2.32	0.00003	−0.2	0.8	1.46	0.66
	Pt−O_1	1.9	2.08	0.00001	−4.2			
	Pt−C	8.3	2.91	0.01000	−1.9			
	Pt−O_2	1.6	3.45	0.00485	−0.6			
fit parameters assuming that only nitrogen neighbors are present								
G4OH−$(Pt^{4+})_{40}$	Pt−Cl	1.9	2.32	0.00036	−0.1	0.9	1.90	0.86
	Pt−N	4.6	2.10	0.00580	−1.0			
	Pt−C	4.0	2.92	0.00190	−0.9			
	Pt−O_2	1.0	3.45	0.00174	−1.1			
fit parameters assuming that both nitrogen and oxygen neighbors are present								
G4OH−$(Pt^{4+})_{40}$	Pt−Cl	2.2	2.32	0.00064	−0.5	0.9	1.54	0.70
	Pt−O_1	1.6	2.07	0.00005	4.4			
	Pt−N	2.1	2.09	0.01000	−9.6			
	Pt−C	8.3	2.91	0.01000	−1.0			
	Pt−O_2	1.2	3.46	0.00296	−1.3			

[a] Notation: R-space fit: $\Delta k = 3.5-15.0$ Å^{-1}, $\Delta r = 1.0-4.5$ Å; standard deviations in fits: $N \pm 20\%$, $R \pm 1\%$, $\Delta\sigma^2 \pm 5\%$, $\Delta E_0 \pm 10\%$; values for $\Delta\sigma^2$ and ΔE_0 are relative to references; all other notations as in Table 2.

functional groups from the dendrimer. Moreover, when no distinction between oxygen (representing aquo ligands) and nitrogen (representing amide or amine functional groups of the dendrimer) was made and only oxygen neighbors were assumed to be present, the sum of nearest neighbors for Pt in the first shell (i.e., Cl and O(N)) was found to be approximately four (Table 3). Similarly, when only nitrogen neighbors were assumed to be present, a total coordination of approximately 6.5 was obtained (Table 3). Taking into account that Pt^{4+} cations usually maintain its octahedral coordination geometry in solutions, we can conclude that the total number of nearest neighbors was underestimated in the first case and slightly overestimated in the second, which was expected based on the literature data discussed in the previous paragraph.[39,40] Therefore, it is proposed that the model with both the Pt−N and Pt−O contributions included provides the most accurate representation of Pt coordination (Table 3). According to this model, at the pH of approximately 2.4 used, on average, the first coordination shell of Pt consists of approximately 2.2 chlorine atoms at a Pt−Cl distance of 2.32 Å, 2.1 nitrogen atoms at a Pt−N distance of 2.09 Å, and 1.6 oxygen atoms at a Pt−O_1 distance of 2.07 Å (Table 3). The similar values obtained for the Pt−O and Pt−N bond distances in our data are not unusual and were observed earlier for cations of other metals (i.e., Cu and Ni) complexed with N- and O-containing ligands such as amino acids.[41] For example, EXAFS structural characterization of bis(glycinato) complexes of Ni^{2+} and Cu^{2+} in water (i.e., $M(gly)_2(H_2O)_2$) revealed the presence of M−O and M−N contributions at bond distances of 2.06 and 2.08 Å, respectively.[42]

The observed Pt−O_1 contributions in our case, once again represent aquo ligands (i.e., H_2O or OH^-), while the Pt−N contributions, in the limits of what was described above, represent structural evidence for the complexation of Pt^{n+} to amide or amine groups of the dendrimer. However, the EXAFS analysis does not allow us to distinguish between nitrogen atoms representing these two different functional groups and, hence, to determine the exact locus of Pt binding within the dendrimer interior. Finally, a comparison of the structural data characterizing G4OH−$(Pt^{4+})_{40}$ (Table 3) with those characterizing H_2PtCl_6/H_2O (Table 2) allows us to conclude that, at the completion of the complexation, approximately one Cl^- ion and one aquo ligand were replaced in the coordination sphere of Pt by two functional groups from the dendrimer.

TABLE 4: Comparison of the White Line Areas and Pt L_3 Edge Energy Positions at Various Stages of the Dendrimer-Derived Catalyst Preparation

sample	white line area	Pt L_3 edge position (eV)
Pt foil	3.8	11564.0
H_2PtCl_6/H_2O	13.1	11567.0
G4OH−$(Pt^{4+})_{40}$	6.8	11564.5
G4OH−$(Pt^{4+})_{40}$ treated with H_2 at room temperature		
for 2 h	6.5	11564.6
for 48 h	6.9	11564.9
for 72 h	6.8	11564.9
H_2PtCl_6/H_2O treated with $NaBH_4$ at room temperature	3.5	11564.0
K_2PtCl_4/H_2O	7.0	11566.0
G4OH−$(Pt^{2+})_{40}$	7.4	11566.0
G4OH−$(Pt^{2+})_{40}$ treated with $NaBH_4$ at room temperature	7.3	11566.0

The distances of 2.91 Å observed for Pt−C contributions and 3.46 Å observed for Pt−O_2 contributions (Table 3) are too long to represent bond formation. Therefore, we suggest that the observed Pt−C contributions represent carbon atoms from the interior of the dendrimer structure. Because the observed Pt−O_2 distance of 3.46 Å is substantially shorter than that determined for the second solvation shell in the aqueous solution of H_2PtCl_6 (Table 2), we suggest that these Pt−O_2 contributions likely represent oxygen atoms from the amide groups located in the interior of the dendrimer structure.

The XANES regions of the spectra obtained were also analyzed to evaluate how the interactions between Pt and the dendrimer influence the electronic structure of Pt. In XANES spectra, the observed band structure for the Pt L_3 edge, commonly called "white line", is indicative of absorption threshold resonances associated with the probability for excitations of $2p_{3/2}$ electrons to unoccupied d states.[43] It is generally assumed that the white line correlates with the electron density of metal atoms, and an increase in the white line area indicates a decrease in the electron density of such atoms.[44] The results shown in Table 4 indicate that the relatively high white line area observed for the H_2PtCl_6/H_2O mixture decreased from 13.1 to 6.8 when the G4OH dendrimer was added to the solution (Table 4). Such a dramatic change in the white line area clearly indicates a strong interaction between platinum and the dendrimer. A possible explanation for this change involves a ligand-

TABLE 5: Structural Parameters Characterizing Interactions of K_2PtCl_4 with a G4OH Dendrimer in an Aqueous Solution[a]

							k^1 variances (%)	
sample	shell	N	R (Å)	$\Delta\sigma^2$ (Å^2)	ΔE_0 (eV)	ϵ_ν^2	im.	abs
fit parameters assuming that only oxygen neighbors are present								
G4OH−$(Pt^{2+})_{40}$	Pt−Cl	0.2	2.32	−0.00465	4.2	0.8	0.77	0.38
	Pt−O_1	2.7	2.07	0.00051	−1.1			
	Pt−C	6.9	2.89	0.01000	1.8			
	Pt−O_2	0.7	3.54	−0.00061	−3.6			
fit parameters assuming that only nitrogen neighbors are present								
G4OH−$(Pt^{2+})_{40}$	Pt−Cl	0.3	2.32	−0.00273	5.3	0.9	0.91	0.46
	Pt−N	4.4	2.11	0.00198	−2.1			
	Pt−C	8.4	2.89	0.00985	1.6			
	Pt−O_2	1.4	3.51	0.00553	−1.1			
fit parameters assuming that both nitrogen and oxygen neighbors are present								
G4OH−$(Pt^{2+})_{40}$	Pt−Cl	0.3	2.32	−0.00163	5.7	0.9	0.91	0.45
	Pt−O_1	1.6	2.08	0.00059	0.7			
	Pt−N	2.1	2.10	0.00286	−3.4			
	Pt−C	7.9	2.89	0.00934	1.5			
	Pt−O_2	1.4	3.51	0.00553	−1.1			

[a] Notation: R-space fit: $\Delta k = 3.5-15.0$ Å^{-1}, $\Delta r = 1.0-4.5$ Å; standard deviations in fits: $N \pm 20\%$, $R \pm 1\%$, $\Delta\sigma^2 \pm 5\%$, $\Delta E_0 \pm 10\%$; values for $\Delta\sigma^2$ and ΔE_0 are relative to references; all other notations as in Table 2.

to-metal charge transfer scheme, which has been commonly observed in other coordination compounds.[45] More specifically, the EXAFS data characterizing the G4OH−$(Pt^{4+})_{40}$ system (Table 3) show that nitrogen atoms of amine and/or amide groups of the dendrimer are likely present in the first coordination shell of platinum, and thus the dendrimer plays the role of a ligand. Therefore, such strong interactions between the dendrimer and platinum can result in transferring of electron density from the dendrimer to platinum, which in turn leads to a decrease in the white line area without a change of coordination geometry, as observed in our results.

The complexation of the Pt^{2+} cations derived from K_2PtCl_4 with the G4OH dendrimer appear to follow a mechanism similar to that observed for Pt^{4+} derived from H_2PtCl_6. Once again, we have taken under consideration various models, with the best fit parameters summarized in Table 5. In the first two models, we have not distinguished between oxygen and nitrogen neighbors in the first coordination shell of Pt, which were modeled with either Pt−O or Pt−N reference files. On the basis of values obtained for the goodness of fit (ϵ_ν^2) and variances for the imaginary and absolute parts of the Fourier transforms, we can conclude that the fit using the Pt−O reference was only slightly better than that using the Pt−N reference. No significant improvement in the statistical parameters was observed when two shells of oxygen and nitrogen scatterers were included in the fit instead of a single shell (Table 5). This result does not necessarily mean that only one type of backscattering atoms is present, but rather points out the small differences in the phase shifts and backscattering amplitudes for nitrogen and oxygen, as explained previously. Similar to the EXAFS data reported for the G4OH−$(Pt^{4+})_{40}$ sample (Table 3), all three models used for the G4OH−$(Pt^{2+})_{40}$ sample (Table 5) indicate that, on average, only 0.3 chlorine ligands remained in the first coordination shell of platinum after the complexation, consistent with the notion that, during complexation, chlorine ligands were replaced by functional groups from the dendrimer. Taking into account that Pt^{2+} complexes have a planar square geometry, we postulate that the models obtained using a single Pt−O or Pt−N shell do not result in realistic coordination numbers. For example, the sum of nearest Cl and O(N) neighbors for Pt^{2+} in the first coordination shell was found to be 2.9 and 4.7 when only Pt−O or Pt−N references were used, respectively. However, the model with the mixture of Pt−O and Pt−N backscatterers leads to a total sum of nearest neighbors of approximately 4, which provides a more realistic result for Pt^{2+} cations having a planar square geometry (Table 5).

No detectable changes were observed in the white line area following complexation of Pt^{2+} with the dendrimer and the formation of the aqueous G4OH−$(Pt^{2+})_{40}$ complex. This result may indicate that the bonds between the G4OH dendrimer and the Pt^{2+} cations are substantially weaker than those between G4OH and Pt^{4+} or that the charge-transfer process is limited in this case. Moreover, we can speculate that the orientation of planar square Pt^{2+} structures toward functional groups of the dendrimer is important during complexation because the functional groups of the dendrimer must be located in plane with the Cl^- and aquo ligands in order to participate in the ligand exchange reaction. In this respect, the complexation of octahedral Pt^{4+} structures should be more favorable due to the presence of additional apex positions for ligands.

Treatment of Pt−PAMAM Complexes with Reducing Agents. Typically, the dendrimer-based templating mechanism described in the literature for the synthesis of metal nanoparticles assumes that all metal cations are located within the dendrimer branches and that the metal nanoparticles formed during reduction remain encapsulated within the dendrimer structure.[2,5,11−13] However, data from some recent literature reports suggest that, depending on the conditions used, this model may be too idealized in the case of Pt. For example, NMR data reported for the complexation of K_2PtCl_4 with PAMAM dendrimers of various generations suggest that as much as 20% of the Pt precursor (for G4OH−$(Pt^{2+})_{40}$) may remain in the aqueous phase of the solution (i.e., not complexed to the dendrimer).[10] The reduction of uncomplexed species will likely lead to the formation of metal aggregates located outside the dendrimer. The precipitation of these colloidal metal particles is arrested by the dendrimer, which acts simply as a steric stabilizer. Furthermore, the valence state of Pt in Pt−PAMAM complexes after treatment with reducing agents remains open to debate. For example, XPS data[46] for G4NH_2−Pt_{30} monolayers supported on Au indicate a Pt ($4f_{7/2}$) binding energy of approximately 73.0 eV, which is considerably higher than that expected for metallic Pt. This high binding energy was attributed to a combination of ligand and quantum size effects.[46] Alternatively, the data can be explained simply by incomplete reduction of the Pt^{n+} cations in the dendrimer.[35]

To further probe these issues, we have collected XANES and EXAFS data for G4OH−$(Pt^{2+})_{40}$ and G4OH−$(Pt^{4+})_{40}$ aqueous

TABLE 6: Structural Parameters Characterizing the Species Formed after the Treatment of the G4OH−$(Pt^{4+})_{40}$ and G4OH−$(Pt^{2+})_{40}$ Aqueous Solutions with $NaBH_4$[a]

							k^1 variances (%)	
sample/treatment	shell	N	R (Å)	$\Delta\sigma^2$ (Å^2)	ΔE_0 (eV)	ϵ_v^2	im.	abs
G4OH−$(Pt^{4+})_{40}$ treated with $NaBH_4$	Pt−O(N)	3.3	2.10	0.00232	−1.9	0.5	1.00	0.50
	Pt−Cl	1.2	2.40	0.00618	−4.4			
	Pt−C	5.1	2.89	0.01000	0.5			
	Pt−O_2	0.7	3.48	0.00226	−0.5			
G4OH−$(Pt^{2+})_{40}$ treated with $NaBH_4$	Pt−O(N)	3.9	2.10	0.00221	−1.4	0.5	0.60	0.30
	Pt−Cl	0.4	2.33	0.00800	2.1			
	Pt−C	7.8	2.92	0.01000	0.1			
	Pt−O_2	1.3	3.51	0.01000	−1.0			
H_2PtCl_6/H_2O treated with $NaBH_4$ [b]	Pt−Pt	3.1	2.71	0.00494	0.0	0.5	0.50	0.27
	Pt−O	6.9	2.41	0.00364	8.4			

[a] Notation: R-space fit: $\Delta k = 3.5-15.0$ Å^{-1}, $\Delta r = 1.0-4.5$ Å; standard deviations in fits: $N \pm 20\%$, $R \pm 1\%$, $\Delta\sigma^2 \pm 5\%$, $\Delta E_0 \pm 10\%$; values for $\Delta\sigma^2$ and ΔE_0 are relative to references; all other notations as in Table 2. [b] R-space fit: $\Delta k = 3.5-15.0$ Å^{-1}, $\Delta r = 1.0-3.0$ Å.

TABLE 7: Structural Parameters Characterizing the Species Formed after the Treatment of the G4OH−$(Pt^{4+})_{40}$ Aqueous Solution with H_2[a]

							k^1-variances (%)	
sample/treatment	shell	N	R (Å)	$\Delta\sigma^2$ (Å^2)	ΔE_0 (eV)	ϵ_v^2	im.	abs
G4OH−$(Pt^{4+})_{40}$ purged with H_2 at 25 °C for 2 h	Pt−Pt	1.3	2.76	0.00113	−3.7	0.9	0.63	0.31
	Pt−O(N)	3.5	2.12	0.00762	−4.7			
G4OH−$(Pt^{4+})_{40}$ purged with H_2 at 25 °C for 48 h	Pt−Pt	2.6	2.77	0.00130	−2.0	0.7	0.96	0.49
	Pt−O(N)	3.3	2.09	0.01000	−1.1			
G4OH−$(Pt^{4+})_{40}$ purged with H_2 at 25 °C for 72 h	Pt−Pt	2.4	2.77	0.00128	−2.0	0.9	0.89	0.34
	Pt−O(N)	3.4	2.09	0.01000	−1.7			

[a] Notation: R-space fit: $\Delta k = 3.5-15.9$ Å^{-1}, $\Delta r = 1.0-3.0$ Å; standard deviations in fits: $N \pm 20\%$, $R \pm 1\%$, $\Delta\sigma^2 \pm 5\%$, $\Delta E_0 \pm 10\%$; values for $\Delta\sigma^2$ and ΔE_0 are relative to references; all other notations as in Table 2.

solutions treated with $NaBH_4$ and H_2. Because, in this case, the main point of interest was the formation of platinum nanoparticles, for simplicity, we no longer attempt to distinguish between nitrogen and oxygen atoms in the first coordination shell and, therefore, the data were analyzed using a Pt−O reference compound. A comparison of the results presented in Tables 5 and 6 indicates that, when $NaBH_4$ was used as the reducing agent for G4OH−$(Pt^{2+})_{40}$, the local environment of Pt in the final solution was nearly identical to that in the starting G4OH−$(Pt^{2+})_{40}$ solution before exposure to the reducing agent. In particular, the first coordination shell of Pt in G4OH−$(Pt^{2+})_{40}$ treated with $NaBH_4$ consists on average of approximately 0.4 chlorine atom at a Pt−Cl distance of 2.33 Å and 3.9 oxygen/nitrogen atoms at a distance of 2.10 Å, representing the first solvation shell aquo ligands and amine or amide functional groups of the dendrimer (Table 6). These results suggest that platinum retained its square planar configuration even after the treatment with $NaBH_4$ and remained attached to the dendrimer.

Similar results were also obtained when the G4OH−$(Pt^{4+})_{40}$ complex was treated with $NaBH_4$ (Table 6). However, in this case, the treatment with $NaBH_4$ led to a further decrease in the number of Cl neighbors and a lengthening/weakening of the remaining Pt−Cl bonds (i.e., 2.4 vs 2.32 Å). Moreover, the analysis of the XANES region of the $NaBH_4$-treated G4OH−$(Pt^{2+})_{40}$ and G4OH−$(Pt^{4+})_{40}$ solutions does not show any substantial changes in the white line area (Table 4), indicating that in both cases platinum remained in cationic form. This conclusion is further reinforced by the EXAFS data (Table 6), demonstrating the absence of high-Z backscatterers (i.e., Pt atoms) in the first coordination shell of platinum for both samples following the treatment with $NaBH_4$. These results allow us to conclude with confidence that treatment of the G4OH−$(Pt^{2+})_{40}$ and G4OH−$(Pt^{4+})_{40}$ solutions with $NaBH_4$ does not lead to the complete reduction of the dendrimer encapsulated Pt cations to a metallic state, nor to the nucleation of Pt atoms into larger clusters or particles.

In contrast, analysis of the EXAFS spectra of a G4OH−$(Pt^{4+})_{40}$ aqueous solution treated with H_2 for 2 h indicates for the first time the presence of a relatively small Pt−Pt contribution with a coordination number of 1.3 at a bond distance of 2.76 Å (Table 7). This result suggests the formation under these conditions of some very small Pt clusters, most likely Pt dimers. Furthermore, approximately 3.5 oxygen/nitrogen atoms were also present in the neighborhood of Pt. Once again, these contributions at a bond distance of 2.12 Å represent the first solvation shell aquo ligands and/or the functional groups (amine and amide) of the G4OH dendrimer (Table 7). The presence of these contributions in the spectra of the H_2-treated sample indicates that Pt remained attached to the dendrimer following this treatment. When longer H_2 treatment times were used, the Pt−Pt coordination number was further increased to approximately 2.6 after 48 h and remained nearly unchanged thereafter (Table 7 and Figure 5). These results suggest the formation of small Pt clusters incorporating on average no more than four Pt atoms. A substantial presence of low-Z backscatterers (i.e., oxygen or nitrogen) in the spectra at a bonding distance of 2.09 Å indicates that these clusters remained in contact with the dendrimer. Furthermore, no Pt−Cl contributions were observed in the EXAFS spectra of the G4OH−$(Pt^{4+})_{40}$ sample after the treatment with H_2, indicating that the treatment with H_2 is more effective for Cl removal than that with $NaBH_4$.

No substantial changes were observed in the white line area even when H_2 was used as the reducing agent for the G4OH−$(Pt^{4+})_{40}$ aqueous solution (Table 4). This result suggests that the small platinum clusters formed remained bonded to the dendrimer and did not undergo complete reduction under these conditions. These observations are consistent with the results of recent theoretical calculations[47] predicting that the reduction

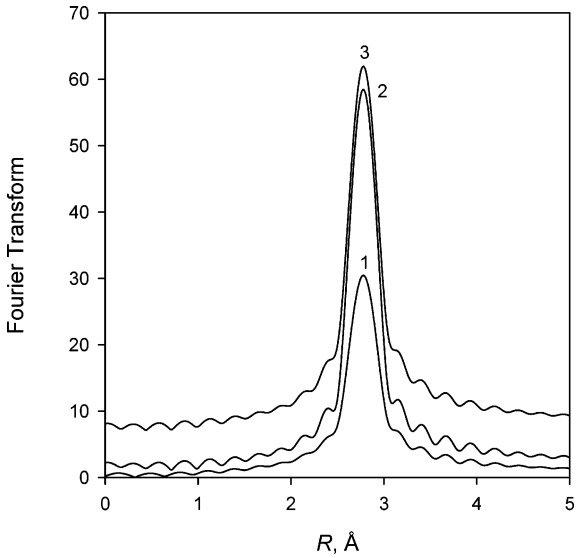

Figure 5. Residual spectra illustrating the first-shell Pt−Pt contributions (i.e., the magnitude of the phase- and amplitude-corrected Fourier transforms (k^3 weighted) of the raw data minus the calculated Pt−O(N) contributions) in G4OH−$(Pt^{4+})_{40}$ complexes treated with H_2 at 25 °C for (1) 2 h, (2) 48 h, and (3) 72 h in an aqueous solution.

of Pt−DNA conjugates should lead to the formation of partially reduced Pt dimers. These dimers are expected to remain strongly bound to the DNA and not easily undergo further reduction.

On the basis of the EXAFS and XANES data discussed above, we conclude that, under the conditions utilized in our experiments, the majority of Pt remained highly dispersed and strongly coordinated to the dendrimer following treatment with the reducing agents. No evidence was obtained for the formation of zero valent Pt nanoparticles. In contrast, when the same experiment was repeated with Pt^{n+} cations in the absence of the dendrimer, the treatment of a H_2PtCl_6 aqueous solution with $NaBH_4$ led to the formation of zero valent colloidal clusters of platinum incorporating on average 3−4 metal atoms, as indicated by the EXAFS and XANES data (Tables 4 and 6). The small Pt cluster size in this colloid is due to the low concentration of Pt in the solution.

Platinum−Dendrimer Nanocomposites Deposited onto γ-Al_2O_3. When the H_2-treated G4OH−$(Pt^{4+})_{40}$ aqueous solution was impregnated onto the γ-Al_2O_3 support and the sample was dried by evacuation at room temperature, Pt−Pt contributions attributed to the first four coordination shells were detected in the EXAFS spectra. The optimized structural parameters characterizing these Pt−Pt contributions are summarized in Table 8. These data clearly demonstrate the formation of platinum nanoparticles under these conditions. They can also be used to estimate the Pt particle size based on known relationships between the average Pt particles size and the Pt−Pt first-shell coordination number.[48] For example, the coordination number of 5.6 determined for the first-shell Pt−Pt contributions following drying of the sample (Table 8) indicates that Pt particles with an average diameter of approximately 10 Å (with nearly 100% of Pt atoms exposed on the surface) were formed under these conditions. The EXAFS data further indicate that these particles remain in close contact with the dendrimer, as evidenced by the presence of Pt−N(O) and Pt−C contributions at 2.03 and 2.14 Å, respectively (Table 8). The formation of Pt nanoparticles for the first time at this stage can be speculatively attributed to the removal of the aquo ligands and the configurational "collapse" of the dendrimer upon deposition on the support and drying. Furthermore, it is possible that upon such a collapse, branches of the dendrimer become "sandwiched" between Pt aggregates, or vice versa, resulting in close proximity of the Pt species with the carbonaceous backbone of the dendrimer, which reflects in the appearance of Pt−C contributions in the EXAFS spectra. Previous ab initio calculations and FTIR measurements for the adsorption of CO have demonstrated that such a collapse indeed takes place.[49−51] Furthermore, this can explain previous TEM "evidence" for the formation of Pt nanoparticles in dendrimer solutions[11] because the TEM protocol requires deposition of the solution on the TEM grid and drying. Hence, the images utilized in the past are representative of a supported system, but not necessarily of the original solution. The EXAFS data of Table 8 further indicate that similar deposition on the γ-Al_2O_3 surface and drying of a G4OH−$(Pt^{4+})_{40}$ nanocomposite that did not previously undergo H_2 treatment in solution do not lead to the formation of any Pt nanoparticles. The Pt^{n+} cations in this sample remained bonded to the Cl ligands and the dendrimer, which indicates that the treatment with H_2 in solution is a necessary condition for Pt nanoparticles to be formed during the subsequent impregnation step.

Removal of the Dendrimer Component. Following drying, the platinum nanoparticles trapped by the dendrimer are shielded from reactants and, consequently, are not catalytically active.[50] Therefore, dendrimer decomposition and removal is an important step in the activation of the catalyst. However, if an advantage in terms of particle size control is to be maintained by this over other conventional catalyst preparation methods, such an activation process should not result in any significant sintering or other changes in the structure of the supported metal nanoparticles. Thermal decomposition is the procedure used so far for this purpose.[35,50,52,53] It was demonstrated by FTIR that the decomposition of dendrimers begins at temperatures as low as 50 °C through the fragmentation of the polymer chains at the amine/amide functional groups.[35,50,52,53] Such a decomposition process can also lead to the formation of small amounts of carbonaceous species on the support surface.[52] XPS data recorded during decomposition of G4OH−Pt films as well as G4OH−Pt/γ-Al_2O_3 nanocomposites indicate that rupture of C═O and C−N bonds in the dendrimer chains takes place at substantially lower temperatures during thermal heating in the presence of Pt, suggesting that Pt encapsulated by the dendrimer is catalyzing the dendrimer decomposition.[35,50] Nevertheless, temperatures as high as 300−400 °C are required to completely remove the dendrimer and render the Pt particles fully accessible for CO adsorption.[50] In addition, it was shown by FTIR and TGA experiments that the decomposition of the G4OH dendrimer proceeds much faster in O_2 than in a nonoxidizing environment such as argon or vacuum.[35,50]

Our EXAFS data summarized in Table 8 provide additional insight to the dendrimer decomposition process, taking place during a combination of oxidation−reduction treatments previously used in the literature to remove the dendrimer fragments from the Pt surface.[50] Following treatment in a 10% O_2/He mixture at 400 °C for 2 h to remove the dendrimer component, the G4OH−$(Pt^{4+})_{40}$/γ-Al_2O_3 sample was purged with He and then reduced in H_2 at 300 °C. The EXAFS data indicate that such an oxidation−reduction treatment leads to an increase in the Pt−Pt first-shell coordination number from 5.6 to 11.2 (Table 8). Calculated coordination numbers for the second, third, and fourth Pt−Pt coordination shells were also increased, indicating sintering of the Pt nanoparticles under these conditions. The first-shell Pt−Pt coordination number of 11.2 corresponds to the formation of metal particles with an average

TABLE 8: Structural Parameters Characterizing the Species Formed after Impregnation of the G4OH−$(Pt^{4+})_{40}$ Nanocomposites on γ-Al_2O_3 and the Subsequent Removal of the Dendrimer Component[a]

sample composition/treatment	shell	N	R (Å)	$\Delta\sigma^2$ (Å^2)	ΔE_0 (eV)	ϵ_v^2	k^1 variances (%) im.	k^1 variances (%) abs
G4OH−$(Pt^{4+})_{40}$ first pretreated with H_2	Pt−Pt_1	5.6	2.76	0.00208	−1.9			
for 2 h and then supported on	Pt−Pt_2	3.4	3.93	0.00539	−4.3	2.2	0.47	0.22
γ-Al_2O_3 and evacuated at 25 °C	Pt−Pt_3	9.1	4.76	0.00632	−3.5			
	Pt−Pt_4	6.3	5.53	0.01000	−7.3			
	Pt−O(N)	2.3	2.03	0.00063	−8.0			
	Pt−C	3.7	2.14	0.00030	0.0			
sample as mentioned above, following	Pt−Pt_1	11.2	2.77	0.00304	−3.7			
treatment with O_2 at 400 °C	Pt−Pt_2	6.0	3.97	0.00039	−9.7			
and H_2 at 300 °C	Pt−Pt_3	15.4	4.78	0.00378	−5.0	3.2	0.87	0.49
	Pt−Pt_4	7.0	5.53	0.00471	−6.4			
	Pt−$O_{support}$	1.8	2.15	0.01000	−5.1			
G4OH−$(Pt^{4+})_{40}$ supported on γ-Al_2O_3	Pt−Cl	2.1	2.35	0.00370	−4.0			
without H_2 pretreatment in solution	Pt−O(N)	5.6	2.13	0.01000	−0.9	2.6	1.40	0.68
and evacuated at 25 °C	Pt−C	7.8	2.91	0.01000	5.1			
	Pt−O(N)[b]	1.7	4.10	−0.00132	4.1			

[a] Notation: R-space fit: $\Delta k = 3.5-15.8$ Å^{-1}, $\Delta r = 1.0-6.0$ Å; standard deviations in fits: $N \pm 20\%$, $R \pm 1\%$, $\Delta\sigma^2 \pm 5\%$, $\Delta E_0 \pm 10\%$; values for $\Delta\sigma^2$ and ΔE_0 are relative to references; all other notations as in Table 2. [b] Contributions represent O(N) atoms from the dendrimer interior not directly bonded to Pt.

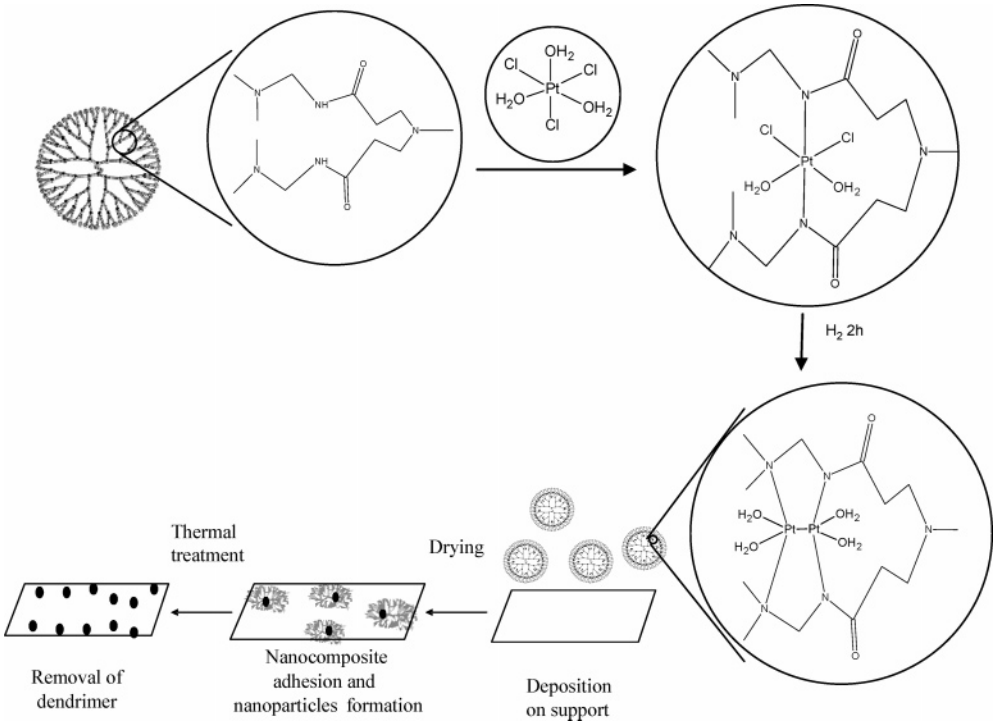

Figure 6. Mechanism for the dendrimer-assisted formation of Pt nanoparticles. The structures shown in circles are provided only for the illustration of the coordination environment of the Pt cations inside the dendrimer and may not represent the exact bonding locations of the Pt cations.

diameter larger than 40 Å. Similar average platinum particle sizes have been observed by TEM for a G4OH−Pt/SiO_2 sample that was exposed to oxidation−reduction treatments at elevated temperatures.[50] The sintering of Pt in our case can be in part attributed to the fact that Pt nanoparticles initially formed during deposition of the G4OH−$(Pt^{4+})_{40}$ on the γ-Al_2O_3 surface remained in contact only with the dendrimer and, therefore, have a higher mobility as compared to Pt atoms directly interacting with the γ-Al_2O_3 surface.[54] Further investigation might lead to an optimized treatment protocol, leading to better Pt dispersion in the final catalyst. In this regard, it is worth considering a low-temperature oxygen plasma treatment as an alternative for removal of dendrimer templates, as reported elsewhere.[55]

The Role of Dendrimers as Templates. The previously proposed mechanism describing the formation of dendrimer encapsulated metal nanoparticles typically includes the complexation of metal cations from a solution by the dendrimer, followed by the reduction of the complexed cations to yield encapsulated nanoparticles. In this mechanism, the dendrimer plays a dual role: to complex up to a certain number of cations from the solution and to stabilize the resulting reduced metal nanoparticles and protect them from aggregation and precipitation.

The EXAFS data reported in this paper allow us to critically reevaluate this mechanism in the case of Pt. The Pt−N contributions observed in the EXAFS spectra after the interaction of H_2PtCl_6 or K_2PtCl_4 with the G4OH dendrimer indeed provide direct structural evidence supporting earlier FTIR[50] and NMR[10] data, indicating that the various amide or amine functional groups located in branches of the dendrimer take part in the complexation of Pt^{n+} cations from the solution. Moreover, the structural data summarized in Tables 3 and 5 indicate that

the dendrimer plays the role of a ligand since, regardless of the platinum precursor used during complexation, the Cl^- ions in the coordination sphere of Pt^{n+} were replaced by functional groups from the dendrimer. Even though we were not able to determine the exact locations for the attachment of the Pt^{n+} cations to the dendrimer, the EXAFS data suggest that the Pt^{n+} cations remained largely isolated from each other throughout the dendrimer interior.

The surprising result is that the Pt^{n+}−N bonds formed between platinum and the dendrimer during complexation appear to be strong and stable. Our attempts to form zero valent Pt nanoparticles following reduction with either $NaBH_4$ or H_2 were not successful. Only when H_2 was used for the reduction of the G4OH−$(Pt^{4+})_{40}$ aqueous solution were some relatively small Pt−Pt contributions with a coordination number of 1.3 at a bond distance of 2.76 Å observed, indicating the formation of Pt dimers. Longer treatments in H_2 further led to the nucleation of Pt into small clusters incorporating on average no more than 4 Pt atoms. Even in these clusters, platinum appears to have remained cationic and coordinated to the dendrimer.

Dendrimers in solutions have an open structure. However, when the metal−dendrimer nanocomposites are deposited on a high surface area support and the solvent is removed, the dendrimer branches tend to collapse and cross-link.[7,53] In the case of γ-Al_2O_3-supported Pt-dendrimer nanocomposites, such a process apparently brings Pt cations closer to each other and favors their clustering toward the formation of nanoparticles, as was observed by EXAFS (Table 8). A schematic of the overall process is shown in Figure 6. The formation of such nanoparticles takes place inside the collapsed dendrimer, and the final size of the formed nanoparticles is likely controlled by the number of metal cations initially stabilized by the dendrimer. The mobility of these dendrimer-covered Pt particles on γ-Al_2O_3 appears to be high, implying that the efficient removal of the dendrimer without Pt sintering is a major challenge for this system that remains to be solved. Despite the fact that Pt promotes the thermal decomposition of dendrimers,[50,52,53] our EXAFS data (Table 8) indicate that simple thermal treatment may be too severe to prevent sintering under the conditions examined.

Conclusions

EXAFS spectroscopy was used to characterize and understand on a molecular level the various steps of the preparation of supported Pt/γ-Al_2O_3 catalysts using G4OH dendrimers as templates. The results indicate that the hydrolysis of two different platinum precursors, namely H_2PtCl_6 and K_2PtCl_4, leads to the formation of $[PtCl_3(H_2O)_3]^+$ and $[PtCl_2(H_2O)_2]$ species, respectively. These species strongly interact with amine and/or amide groups in the interior of the G4OH dendrimer. Such interactions lead to transfer of electron density from the dendrimer to platinum and to the replacement of Cl^- ions in the coordination sphere of Pt^{n+} by functional groups from the dendrimer, indicating that the dendrimer plays the role of a ligand. No substantial electronic or structural changes were observed when both G4OH−$(Pt^{4+})_{40}$ and G4OH−$(Pt^{2+})_{40}$ aqueous solutions were treated with $NaBH_4$ at room temperature, indicating that complete reduction of the Pt^{n+} cations and the formation of metallic Pt nanoparticles does not take place under these conditions. The formation of Pt dimers or extremely small clusters incorporating on average no more than four platinum atoms was observed when the G4OH−$(Pt^{4+})_{40}$ system was treated with H_2. These dimers and clusters remained strongly bonded to the dendrimer and are most likely cationic in nature. The formation of zero valent Pt nanoparticles eventually took place following the impregnation of the H_2-treated G4OH−$(Pt^{4+})_{40}$ nanocomposites on a γ-Al_2O_3 surface and subsequent drying, presumably because the removal of the solvent leads to the collapse of the dendrimer branches and clustering of the Pt cations. Subsequent thermal treatments in O_2/H_2 atmospheres lead to sintering of the Pt particles, indicating that the Pt nanoparticles initially formed have high mobility on the dendrimer surface. Thus, the removal of the dendrimer without substantial sintering of the metal component remains a challenge that needs to be solved if this approach is going to be used in heterogeneous catalyst synthesis.

Acknowledgment. This research was supported in part by the National Science Foundation (NSF NIRT Award CTS-0103135) and by the U.S. Department of Energy (DE-FG02-05ER15731). Use of the National Synchrotron Light Source, Brookhaven National Laboratory, was supported by the U. S. Department of Energy, Office of Science, Office of Basic Energy Sciences, under contract no. DE-AC02-98CH10886. Portions of this research were also carried out at the Stanford Synchrotron Radiation Laboratory, a national user facility operated by Stanford University on behalf of the U.S. Department of Energy, Office of Basic Energy Sciences. We are grateful to the beamline staff at both facilities for their assistance. The EXAFS data were analyzed with the XDAP software developed by Vaarkamp et al.[19]

References and Notes

(1) Alexeev, O.; Gates, B. C. *Top. Catal.* **2000**, *10*, 273.
(2) Zhao, M.; Sun, L.; Crooks, R. M. *J. Am. Chem. Soc.* **1998**, *120*, 4877.
(3) Tomalia D. A.; Naylor, A. M.; Goddard, W. A. *Angew. Chem., Int. Ed. Engl.* **1990**, *29*, 138.
(4) Tomalia, D. A.; Baker, H.; Dewald, J.; Hall, M.; Kallos, G.; Martin, S.; Roeck, J.; Ryder, J.; Smith, P. *Polym. J.* **1985**, *17*, 117.
(5) Scott, R. W. J.; Wilson, O. M.; Crooks, R. M. *J. Phys. Chem. B* **2005**, *109*, 692.
(6) Ooe, M.; Murata, M.; Mizugaki, T.; Ebitani, K.; Kaneda, K. *Nano Lett.* **2002**, *2*, 999.
(7) Lang, H.; Maldonado, S.; Stevenson, K. J.; Chandler, B. D. *J. Am. Chem. Soc.* **2004**, *126*, 1294.
(8) Chung Y.; Rhee H. *J. Mol. Catal. A: Chem.* **2003**, *206*, 291.
(9) Roucoux, A.; Schulz, J.; Patin, H. *Chem. Rev.* **2002**, *102*, 3757.
(10) Pellecchia P. J.; Gao, J.; Gu, Y.; Ploehn, H. P.; Murphy, C. J. *Inorg. Chem.* **2004**, *43*, 1421.
(11) Crooks, R. M.; Zhao, M.; Sun, L.; Chechik, V.; Yeung, L. K. *Acc. Chem. Res.* **2001**, *34*, 181.
(12) Esumi, K.; Suzuki, A.; Aihara, N.; Usui, K.; Torigoe, K. *Langmuir* **1998**, *14*, 4, 3157.
(13) Gröhn, F.; Bauer, B. J.; Akpalu, Y. A.; Jackson, C. L. Amis, E. J. *Macromolecules*, **2000**, *33*, 6042.
(14) Jentoft, R. E.; Deutsch, S. E.; Gates, B. C. *Rev. Sci. Instrum.* **1996**, *67*, 2111.
(15) Marcos, E. S.; Gil, M.; Martínez, J. M., Muñoz-Páez, A. *Rev. Sci. Instrum.* **1994**, *65*, 2153.
(16) Teo, B. K. *J. Am. Chem. Soc.* **1981**, *103*, 3990.
(17) Teo, B. K.; Lee, P. A. *J. Am. Chem. Soc.* **1979**, *101*, 2815.
(18) Duivenvoorden, F. B. M.; Koningsberger, D. C.; Uh, Y. S.; Gates, B. C. *J. Am. Chem. Soc.* **1986**, *108*, 6254.
(19) Vaarkamp, M.; Linders, J. C.; Koningsberger, D. C. *Physica B* **1995**, *208−209*, 159.
(20) Koningsberger, D. C. In *Synchrotron Techniques in Interfacial Electrochemistry;* Melendres, C. A., Tadjeddine, A., Eds.; Kluwer: Dordrecht, 1994.
(21) Stern, E. A. *Phys. Rev. B* **1993**, *48*, 9825.
(22) Brigham, E. O. *The Fast Fourier Transform*; Prentice Hall: Englewood Cliffs, NJ, 1974.
(23) Kirlin, P. S.; van Zon, F. B. M.; Koningsberger, D. C.; Gates, B. C. *J. Phys. Chem.* **1990**, *94*, 8439.
(24) van Zon, J. B. A. D.; Koningsberger, D. C.; van't Blik, H. F. J.; Sayers, D. E. *J. Chem. Phys.* **1985**, *82*, 5742.

(25) Vaarkamp, M. Ph.D. Thesis, Eindhoven University, Eindhoven, The Netherlands, 1993.

(26) Lytle, F. W.; Sayers, D. E.; Stern, E. A. *Physica B* **1988**, *158*, 701.

(27) Koningsberger, D. C.; Mojet, B. L.; van Dorssen, G. E.; Ramaker, D. E. *Top. Catal.* **2000**, *10*, 143.

(28) Spieker W. A.; Liu, J.; Kropf, J.; Miller, J. T.; Regalbuto, J. R. *Appl. Catal., A* **2002**, *232*, 219.

(29) Miolati, A.; Pendini, U. *Z. Anorg. Chem.* **1903,** *33*, 251.

(30) Gmelin, L.; Meyer, R. J. *Gmelins Handbuch der Anorganischen Chemie*; Verlag Chemie: Weinheim, 1939.

(31) Boitiaux, J. P.; Deves, J. M.; Didillon, B.; Marcilly, C. R. In *Catalytic Naphtha Reforming, Science and Technology*; Antos, G. J., Aitani, A. M., Parera J. M., Eds.; Marcel Dekker: New York, 1995; p 79.

(32) Ayala, R.; Marcos, E. S.; Díaz-Moreno, S.; Sole, V. A.; Muñoz-Páez, A. *J. Phys. Chem. B* **2001,** *105*, 7588.

(33) Hellquist, B.; Bengtsson, L. A.; Holmberg, B.; Hedman, B.; Persson, I.; Elding, L. I. *Acta Chem. Scand.* **1991**, *45*, 449.

(34) Lederer, M.; Leipzig-Pagani, E. *Anal. Chim. Acta* **1997**, *350*, 203.

(35) Ozturk, O.; Black, T. J.; K. Perrine, K.; K. Pizzolato, K.; Williams, C. T.; Parsons, F. W.; Ratliff, J. S.; Gao, J.; Murphy, C. J.; Xie, H.; Ploehn, H. J.; Chen, D. A. *Langmuir* **2005,** *21*, 3998.

(36) Koningsberger, D. C.; Prins, R. *X-ray Absorption: Principles, Applications, Techniques of EXAFS, SEXAFS and XANES*; Wiley: New York, 1988.

(37) Oudenhuijzen, M. K.; Kooyman, P. J.; Tappel, B.; van Bokhoven, J. A.; Koningsberger, D. C. *J. Catal.* **2002**, *205*, 135.

(38) Clark, K.; Penner-Hahn, J. E.; Whittaker, M.; Whittaker, J. W. *Biochemistry* **1994**, *33*, 12553.

(39) Muñoz-Páez, A.; Koningsberger, D. C. *J. Phys. Chem.* **1995**, *99*, 4193.

(40) Vaarkamp, M.; Koningsberger, D. C. In *Handbook of Heterogeneous Catalysis*; Ertl, G., Knözinger, H., Weitkamp, J., Eds.; VCH: Weinheim, 1997; p 475.

(41) Ohtaki, H.; Masuda, H. In *Macromolecular Complexes: Dynamic Interactions and Electronic* Processes; Tsuchida, E., Ed.; VCH: New York, 1991; p 175.

(42) Ozutsumi, K.; Yamaguchi, T.; Ohtaki, H.; Tohji, K.; Udagawa, Y. *Bull. Chem. Soc. Jpn.* **1995**, *58*, 2789.

(43) Iwasawa, Y. *X-ray Absorption Fine Structure for Catalysts and Surfaces*; World Scientific: Singapore, 1996.

(44) Sinfelt, J. H.; Meitzner, G. D. *Acc. Chem. Res.* **1993**, *26*, 1.

(45) Miesser, G. L.; Tarr, D. A. *Inorganic Chemistry*, 3rd ed.; Pearson Prentice Hall: New Jersey, 2004; p 379.

(46) Ye, H.; Scott, R. W. J.; Crooks, R. M. *Langmuir* **2004,** *20*, 2915.

(47) Ciacchi, L. C.; Mertig, M.; Seidel, R.; Pompe, W.; De Vita, A. *Nanotechnology* **2003**, *14*, 840.

(48) Kip, B. J.; Duivenvoorden, F. B. M.; Koningsberger, D. C.; Prins, R. *J. Catal.* **1987**, *105*, 26.

(49) Tarazona-Vasquez, F.; Balbuena, P. B. *J. Phys. Chem. B* **2004**, *108*, 15992.

(50) Deutsch, D. S.; Lafaye, G.; Liu, D.; Chandler, B.; Williams, C. T.; Amiridis, M. D. *Catal. Lett.* **2004**, *97*, 139.

(51) Maiti, P. K.; Cagin, T.; Lin, S.-T.; Goddard, W. A. *Macromolecules* **2005**, *38*, 979.

(52) Lafaye, G.; Williams, C. T.; Amiridis, M. D. *Catal. Lett.* **2004**, *96*, 43.

(53) Lang, H.; May, R. A.; Iversen, B. L.; Chandler, B. D. *J. Am. Chem. Soc.* **2003**, *125*, 14832.

(54) Alexeev, O.; Kim, D.-W.; Graham, G. W.; Shelef, M.; Gates, B. C. *J. Catal.* **1999**, *185*, 170.

(55) Boyen, H.-G.; Kästle, G.; Weigl, F.; Koslowski, B.; Dietrich, C.; Ziemann, P.; Spatz, J. P.; Riethmüller, S.; Hartmann, C.; Moller, M.; Schmid, G.; Garnier M. G.; Oelhafen, P. *Science* **2002**, *297*, 1533.